Paleoceanography and Paleoclimatology

RESEARCH ARTICLE
10.1029/2020PA003917

Special Section:
The Miocene: The Future of the Past

Provenance and Weathering of Clays Delivered to the Bay of Bengal During the Middle Miocene: Linkages to Tectonics and Monsoonal Climate

Lisa Bretschneider[1], Ed C. Hathorne[1], Huang Huang[1], Julia Lübbers[2], Karlos G. D. Kochhann[2,3], Ann Holbourn[2], Wolfgang Kuhnt[2], Rasmus Thiede[2], Daniel Gebregiorgis[4], Liviu Giosan[5], and Martin Frank[1]

[1]GEOMAR Helmholtz Centre for Ocean Research Kiel, Kiel, Germany, [2]Institute of Geosciences, Christian-Albrechts-University Kiel, Kiel, Germany, [3]Geology Graduate Program, UNISINOS University, São Leopoldo, Brazil, [4]Department of Geosciences, Georgia State University, Atlanta, GA, USA, [5]Woods Hole Oceanographic Institution, Woods Hole, MA, USA

Abstract Tectonics and regional monsoon strength control weathering and erosion regimes of the watersheds feeding into the Bay of Bengal, which are important contributors to global climate evolution via carbon cycle feedbacks. The detailed mechanisms controlling the input of terrigenous clay to the Bay of Bengal on tectonic to orbital timescales are, however, not yet well understood. We produced orbital-scale resolution geochemical records for International Ocean Discovery Program Site U1443 (southern Bay of Bengal) across five key climatic intervals of the middle to late Miocene (15.8–9.5 Ma). Our new radiogenic Sr, Nd, and Pb isotope time series of clays transported to the Ninetyeast Ridge suggest that the individual contributions from different erosional sources overall remained remarkably consistent during the Miocene despite major tectonic reorganizations in the Himalayas. On orbital timescales, however, high-resolution data from the five investigated intervals show marked fluctuations of all three isotope systems. Interestingly, the variability was much higher within the Miocene Climatic Optimum (around 16–15 Ma) and across the major global cooling (~13.9–13.8 Ma) until ~13.5 Ma, than during younger time intervals. This change is attributed to a major restriction on the supply of High Himalayan erosion products due to migration of the peak precipitation area toward the frontal domains of the Himalayas and the Indo-Burman Ranges. The transient excursions of the radiogenic isotope signals on orbital timescales most likely reflect climatically driven shifts in monsoon strength.

Key Points:
- A consistent mix of clay sources contributed to the Bay of Bengal throughout the middle to late Miocene
- A marked change in detrital Sr, Nd, and Pb isotope variability at 13.5 Ma was related to Miocene global cooling
- Transient orbital-scale fluctuations in clay source most likely reflect changes in monsoon intensity

Supporting Information:
- Supporting Information S1
- Table S1
- Table S2

Correspondence to:
L. Bretschneider,
lbretschneider@geomar.de

Citation:
Bretschneider, L., Hathorne, E. C., Huang, H., Lübbers, J., Kochhann, K. G. D., Holbourn, A., et al. (2021). Provenance and weathering of clays delivered to the Bay of Bengal during the middle Miocene: Linkages to tectonics and monsoonal climate. *Paleoceanography and Paleoclimatology*, *36*, e2020PA003917. https://doi.org/10.1029/2020PA003917

Received 19 MAR 2020
Accepted 18 NOV 2020
Accepted article online 25 NOV 2020

1. Introduction

The South Asian monsoon (SAM) influences the lives of more than a billion people but remains difficult to predict. It is thus crucial to understand how the monsoon behaves under different boundary conditions such as a warmer world with reduced continental ice cover. Many studies have focused on the Late Quaternary glacial-interglacial cycles to reconstruct how monsoon strength, weathering intensity, and global climate have been linked on orbital timescales (e.g., Ahmad et al., 2005; Colin et al., 1999; Gebregiorgis et al., 2018; Joussain et al., 2016; Li et al., 2018; Wilson et al., 2015), but there are fewer studies of warmer periods in the geological past. Since the monsoon is thought to have initiated during the warmer than present Miocene (Clift et al., 2008), this period of time offers a unique window into past monsoon variability and its controlling factors. Studies that investigated the relationship between variations of the SAM and the erosional regime during the Miocene period were conducted at low time resolution (e.g., France-Lanord et al., 1993: Myr timescale; Banerjee et al., 2019: ~500 kyr resolution) and thus do not allow insights into the links between orbital-scale climate variability and monsoon strength.

The continuous sediment archive recovered at International Ocean Discovery Program (IODP) Site U1443 in the Bay of Bengal (Figure 1) now allows a much more detailed study. Lübbers et al. (2019) established a high-resolution benthic stable isotope record from 13.5 to 8.2 Ma for Site U1443, which provides the climatic and stratigraphic framework to reconstruct Himalayan silicate weathering and its relationship to changes of the SAM and climate during the Miocene based on radiogenic isotope compositions of the clay size fraction. Since tectonics, climate, erosion, type, and intensity of weathering and monsoon strength can all affect the

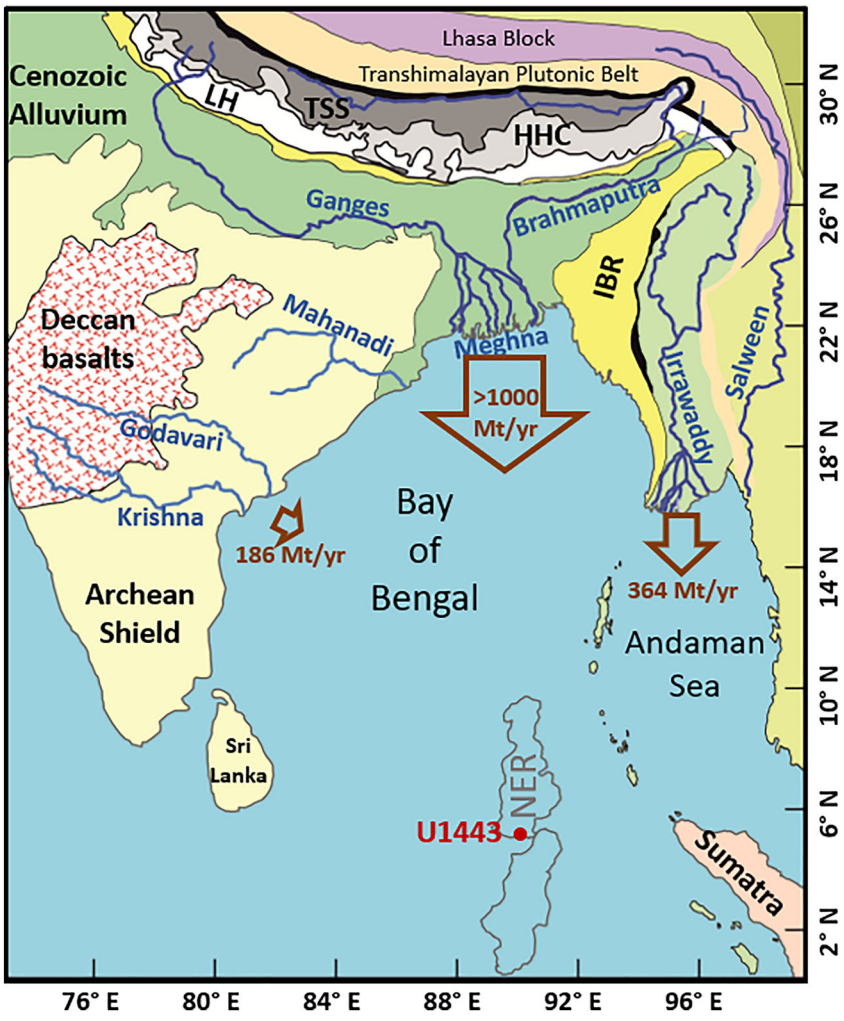

Figure 1. Map of the Bay of Bengal modified from Ali et al. (2021). The location of IODP Site U1443 on the Ninetyeast Ridge (NER) is marked. The major continental river systems are indicated as well as the major geological units: LH = Lesser Himalayas, TSS = Tethyan Sedimentary Series, HHC = High Himalayan Crystalline, and IBR = Indo-Burman Ranges. The arrows indicate modern sediment fluxes from major rivers (Milliman & Syvitski, 1992; Robinson et al., 2007).

detrital isotope signatures on different time scales, our approach is to disentangle the different factors using higher temporal resolution records than in previous work to advance our understanding of the major controls of past SAM intensity.

The Bay of Bengal receives large freshwater and sediment inputs from the rivers draining the Himalaya (Ganges, Brahmaputra, and Meghna), the Indo-Burman Ranges and the Arakan coast (Irrawaddy), and the Indian Peninsula (Godavari, Krishna, and Mahanadi) (Figure 1). The sediments deposited in the Bay of Bengal mainly originate from Himalayan erosion and have formed the Bengal Fan, the world's largest submarine fan with a sediment volume of $12.5 * 10^6$ km^3 (Curray et al., 2003). The Bengal Fan has existed since at least early Miocene times (Derry & France-Lanord, 1996; France-Lanord et al., 1993), and its deposits provide a record of the erosion and weathering history of the surrounding mountain belts, as a consequence of the continental Indian-Eurasian collision and the resulting uplift history of the Himalayas (Colin et al., 1999; France-Lanord et al., 1993). In the modern system, 95% of the volume of sediments is transported to the Bay of Bengal during peak monsoon precipitation (Singh et al., 2007), and thus, the variability of erosion intensity and deposition rates is directly related to changes in monsoonal precipitation. The erosion of the Himalayas is considered to be fundamental for regulating Earth's climate because the

sequestration of CO_2 through enhanced silicate weathering and the burial of organic carbon in the fan result in lower global temperatures (France-Lanord & Derry, 1997; Galy et al., 2007, 2010; Raymo, 1994; Raymo & Ruddiman, 1992).

Radiogenic Sr, Nd, and Pb isotope compositions of detrital materials transported to the central Bay of Bengal vary as a function of the age and the geological history of the continental rocks in the hinterland and, therefore, serve as reliable tracers of the sediment sources (Ahmad et al., 2005; Colin et al., 1999). The continental lithologies surrounding the Bay of Bengal constrain the possible end-members for the mixture of sediment deposited at Site U1443. Within the Himalayas, at least four main lithologies are likely sources: The Lesser Himalaya (LH), the High Himalayan Crystalline (HHC), the Tethyan Sedimentary Series (TSS), and the Transhimalayan Plutonic Belt (TPB) (France-Lanord & Le, 1988; Galy et al., 1996; Gansser, 1964; LeFort, 1975; Singh & France-Lanord, 2002). Another important source are the Indo-Burman Ranges (IBR), which are drained by the Irrawaddy River (Giosan et al., 2018). Based on the mixture of these distinct sediment source signatures in the Bay of Bengal, the location of highest monsoon precipitation as well as erosional and tectonic changes can be reconstructed. Sr and Pb isotope compositions are additionally influenced by fractionation during weathering and transport due to large variations in the isotope composition of different mineral phases and differences in their resistance to weathering (Ali et al., 2015; Blum et al., 1993; Tütken et al., 2002). These signals can potentially provide useful information on prevailing types and intensities of weathering and thus help reconstructing past weathering regimes.

The Miocene epoch (23.03–5.33 Ma) was characterized by pronounced global climatic changes. The Miocene Climatic Optimum (MCO, ~17 to 15 Ma) was a warm period with global annual mean temperatures ~3°C higher than today, based on proxy data constraining land and sea surface temperatures (You et al., 2009). Taking into account variations in global tectonic boundary conditions, Miocene climate reconstructions thus allow insights into the ability of climate models to simulate warm climates, comparable to those the Earth may experience in the near future (Henrot et al., 2017). The MCO was followed by a stepwise cooling trend with development of a permanent Antarctic ice sheet after ~13.8 Ma (e.g., Holbourn et al., 2005) that was associated with a marked decrease in atmospheric CO_2 (Foster et al., 2012). Miocene climatic changes and tectonic events may have been closely linked, since erosion intensity increases with the amount of precipitation, which in turn influenced relief and exhumation rates (Deng et al., 2019). Furthermore, Raymo (1994) proposed that increased silicate weathering, as well as organic carbon burial, promotes CO_2 drawdown and may have led to the global cooling in the middle Miocene.

The study by Allen and Armstrong (2012) summarized the main tectonic events in the Himalayan-Tibetan region during the Miocene, which comprised a reorganization of the thrusting, which propagated south from the Main Central Thrust (MCT). Large changes in tectonic regime have been inferred for the middle Miocene, starting with synchronous ductile shear along the South Tibetan Detachment System and the MCT (Burchfiel et al., 1992; Hodges et al., 1998; Kellett et al., 2009; Searle et al., 2008), contemporaneous with leucogranite generation and rapid exhumation (Catlos et al., 2004; Thiede et al., 2004). This was followed by the onset of approximately N-S oriented normal faulting in southern Tibet and thrusting south of the MCT (Allen & Armstrong, 2012; Molnar & Tapponnier, 1978), as well as a decrease in exhumation rates of the High Himalayas at ~16 Ma (Najman et al., 2009; Thiede et al., 2009). These processes played an important role in determining which Himalayan rocks were exposed and were thus subject to erosion during particular periods of time. Changes in the tectonically induced exposure of different rock types are therefore expected to be reflected by source changes of the eroded material in the Bay of Bengal sediments. Despite this, previous studies have shown that the sources of sediments in the Bay of Bengal have remained overall similar since at least the early Miocene (Ali et al., 2021; Bouquillon et al., 1990; France-Lanord et al., 1993). However, on orbital timescales, significant variations in the provenance and grain size of sediments have been observed and attributed to climate and monsoon changes (Ahmad et al., 2005; Bookhagen et al., 2006; Clift et al., 2008; Colin et al., 1999; Tripathy et al., 2011). Over the most recent glacial-interglacial cycles, the interglacials were generally dominated by a strong summer monsoon, while the glacials were drier and suggested to have been characterized by a stronger winter monsoon (Ahmad et al., 2005; Galy et al., 2008; Joussain et al., 2016; Li et al., 2018; Tripathy et al., 2011; Wilson et al., 2015). However, in detail, this relationship is not always as clear and periods with strong monsoons were also recognized during glacials (Bolton et al., 2013; Gebregiorgis et al., 2018).

Here we follow a similar high-resolution approach to the glacial-interglacial studies, to reconstruct both long and short-term monsoon variability. However, instead of using Bengal fan sediments, which are often disturbed and discontinuous due to the occurrence of turbidites (e.g., Derry & France-Lanord, 1996; Galy et al., 1996, 2010), we analyze the continuous sediment record of the crest of the Ninetyeast Ridge (NER). Moreover, we focus on the detrital clay size to minimize mineral sorting effects, which may occur during transport. Since the time-consuming preparation of the samples limits the number of analyses of radiogenic isotopes, we focus on orbital-scale variability during five selected Miocene key climatic intervals to better constrain the roles of tectonics and global climate in driving regional monsoon intensity and erosion and to discuss potential interactions and feedbacks between them. The selected intervals include the central part of the MCO (15.8–15.3 Ma), two global cooling steps from 14 to 13.5 and 13.3 to 12.8 Ma, the event of peak warmth at 11–10.5 Ma and an interval marking the transition from ~100 kyr periodicity to the dominant 41 kyr variability in benthic $\delta^{18}O$ (10–9.5 Ma).

2. Materials and Methods

Our study is based on sediments of IODP Site U1443 (Latitude 5°23′N; Longitude 90°21′E, water depth: ~2,930 m), cored with the RV *JOIDES Resolution* during IODP Expedition 353 in December 2014. Site U1443 was a redrill of nearby Ocean Drilling Program (ODP) Site 758 and located on the crest of the NER in the southern Bay of Bengal. This ridge-top location ensured a slow and continuous sedimentation and prevented the deposition of disturbed sedimentary sequences typically associated with transport processes on the Bengal Fan (Clemens et al., 2016). The average sedimentation rates during the Miocene varied between 0.41 cm/kyr in the late to middle Miocene and 0.81 cm/kyr in the early Miocene to Oligocene. Four holes were combined to form a splice comprising sediments from the Oligocene to the late Pleistocene. The recovered sediment is a nannofossil ooze with varying abundances of detrital clays, foraminifers, and authigenic carbonates (Clemens et al., 2016). The Miocene samples investigated in this study span a composite depth between 125.88 and 152.78 m below seafloor. The age model is based on the isotope stratigraphy of Lübbers et al. (2019) for the intervals younger than 13.5 Ma and of K. Kochhann (supporting information Table S1, personal communication, March 2020) for the intervals older than 13.5 Ma. The Irrawaddy samples were collected during field expeditions to the Irrawaddy delta in 2016 and 2017 (for further information see Giosan et al., 2018).

The sediment samples were washed over a 63 μm sieve and the fine fraction collected in 3 L plastic bags. While the coarser fraction was used for micropaleontology, the fine fraction was freeze-dried and leached to remove all authigenic Fe-Mn oxyhydroxides. The leaching procedure was modified from Gutjahr et al. (2007). Briefly, ~2 g of fine sediments were washed with deionized water, leached step by step with a 0.05 M hydroxylamine hydrochloride—15% acetic acid—0.03 M Na-EDTA solution, buffered to pH 4 with analytical grade NaOH, and fully decarbonated with 40% acetic acid. Having been washed again with deionized water, the clay fraction was separated using a centrifuge-based Atterberg method.

For the Sr, Nd, and Pb isotope analyses, the clay fraction was then dried at low temperature (<45°C) in an oven. For the Irrawaddy samples, both clay and >2 μm fractions were dried and digested. About 100 mg of the dried silicate clays (and silts) were completely digested using alkaline fusion ($NaOH\text{-}Na_2O_2$), as described in Bayon et al. (2009) but without addition of TiO_2, Fe_2O_3, or Tm, and then further dissolved in 6 M HCl. To separate and purify Nd, Sr, and Pb, standard ion chromatographic procedures were applied (Cohen et al., 1988; Galer & O'Nions, 1989; Pin & Zalduegui, 1997). For Nd, first the REEs (including Nd) were separated using a cation exchange resin (Bio-Rad AG 50W-X8, 200–400 mesh), while most matrix elements were discarded. The Nd was then separated from the other REEs using Ln-spec resin (50–100 μm). Pb and Sr were separated using AG1-X8 (100–200 μm) and Sr-Spec resin, respectively. Sr isotope and some Nd isotope measurements were performed on a Nu Plasma high-resolution multi-collector inductively coupled plasma mass spectrometer (MC-ICP-MS) at GEOMAR while most Nd and all Pb isotope analyses were carried out on a Thermo Scientific Neptune Plus MC-ICP-MS at GEOMAR.

Nd isotope ratios were corrected for instrumental mass bias using a $^{146}Nd/^{144}Nd$ of 0.7219 (Vance & Thirlwall, 2002) and were normalized to the accepted values of the JNdi-1 standard (0.512115; Tanaka et al., 2000). The Nd isotope ratios are reported as $\varepsilon_{Nd}(0)$ values = $((^{143}Nd/^{144}Nd)_{sample}/(^{143}Nd/^{144}Nd)_{CHUR} - 1) \times 10^4$ with CHUR being the Chondritic Uniform Reservoir and ($^{143}Nd/$

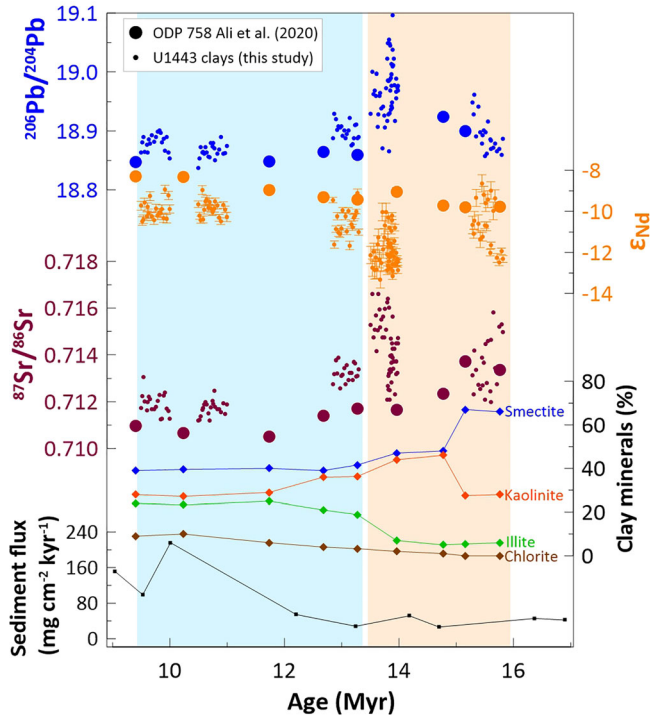

Figure 2. Radiogenic Pb, Sr, and Nd isotope compositions of the U1443 clay samples for the five investigated Miocene time intervals. The larger symbols represent part of the ODP Site 758 low-resolution clay record by Ali et al. (2021). The light orange shaded interval marks high variability of the radiogenic isotopes while the blue shaded interval reflects the low variability after the first Miocene cooling interval. The relative abundances of the clay minerals smectite, kaolinite, illite, and chlorite from ODP Site 758 (Ali et al., 2021) are shown, as well as the sediment flux record of ODP Site 758 (Hovan & Rea, 1992; recalculated by Ali et al., 2021).

$^{144}Nd)_{CHUR}$ = 0.512638 (Jacobsen & Wasserburg, 1980). Procedural blanks for Nd were <0.5 ng and thus below 0.5% of the total amount of Nd in the samples. Separate digestions and measurements of USGS reference material BHVO-2 (n = 8) gave a mean ε_{Nd} value of 6.75 ± 0.24, which agrees well with the mean value (6.65 ± 0.60) compiled by the GeoReM database (Jochum et al., 2016).

The instrumental mass bias of Sr isotopic measurements was corrected using a $^{88}Sr/^{86}Sr$ of 0.1194 (Steiger & Jäger, 1977) and normalized to the NIST SRM 987 $^{87}Sr/^{86}Sr$ of 0.710245. Procedural blanks were on average 50 ng, contributing between 0.7 and 8.8% of the total Sr signal. This rather high contribution originated from the NaOH and NaO_2 used for the alkaline fusion. To correct for the blank contributions, samples of the reagents were regularly digested and measured for concentrations (n = 15). These were later combined and measured for their isotopic composition. The blank contributions were then removed from the Sr sample signals via mass balance calculations. Repeated digestions and measurements of USGS reference material BHVO-2 (n = 12) gave a mean $^{87}Sr/^{86}Sr$ value of 0.70363 ± 0.00013, which is in good agreement with the GeoReM average value of 0.70348 ± 0.00006.

The mass bias correction for the Pb isotope measurements was carried out by doping the samples with the NIST997 Tl standard solution (Pb/Tl ~ 4) (Belshaw et al., 1998; White et al., 2000). Since Tl and Pb fractionate slightly differently during ionization (Vance & Thirlwall, 2002), $^{205}Tl/^{203}Tl$ was adjusted on a session-by-session basis in order to match accepted SRM 981 Pb isotope compositions ($^{206}Pb/^{204}Pb$ = 16.9416, $^{207}Pb/^{204}Pb$ = 15.4998, and $^{208}Pb/^{204}Pb$ = 36.7249; Baker et al., 2004). Repeated processing and analysis of USGS reference material BHVO-2 (n = 6) gave mean values (±2 standard deviations) of 18.619 ± 0.090, 15.536 ± 0.019, and 38.219 ± 0.052 for $^{206}Pb/^{204}Pb$, $^{207}Pb/^{204}Pb$, and $^{208}Pb/^{204}Pb$, respectively. These Pb isotope values agree well with those previously measured for BHVO-2 (n = 44, 18.637 ± 0.073, 15.528 ± 0.045, and 38.223 ± 0.103; GeoReM database). Procedural blanks for Pb were <70 pg and contributed less than 0.1% of the total amount of Pb in the samples.

In order to identify cyclic changes in contributions from the source areas reflected by the radiogenic isotope compositions of the clay fractions, spectral analyses of the records were performed on unevenly spaced time series using REDFIT (Schulz & Mudelsee, 2002).

3. Results

The ε_{Nd}, $^{87}Sr/^{86}Sr$ and Pb isotope compositions ($^{206}Pb/^{204}Pb$, $^{207}Pb/^{204}Pb$, $^{208}Pb/^{204}Pb$, $^{207}Pb/^{206}Pb$, and $^{208}Pb/^{206}Pb$) of the silicate clay fraction are shown in Figure 2 and supporting information Table S2. The ε_{Nd} values range from −13.3 to −8.6 and exhibit highest variability during the MCO and the 14–13.5 Ma interval, which comprises the global cooling step at ~13.9–13.8 Ma. The least radiogenic ε_{Nd} values (−13.3) were found at 13.7 Ma. The $^{87}Sr/^{86}Sr$ compositions vary between 0.71119 and 0.71661, also showing the highest fluctuations and highest values, in the two older intervals. The youngest two investigated intervals after the cooling only show minor variability and overall lower values, ranging from 0.71119 to 0.71306. $^{206}Pb/^{204}Pb$ values vary between 18.84 and 19.10 and exhibit a clear radiogenic peak and the highest variability at the beginning of cooling at ~14 Ma.

To evaluate potential grain size effects, differences in Sr, Nd, and Pb isotopic compositions of the same samples between clay (<2 μm) and silt (>2 μm) fractions from the Irrawaddy delta (Giosan et al., 2018) were analyzed (Figure 3). The clay size Irrawaddy samples show systematically more radiogenic Nd isotope signatures than the silt size samples (a difference of 2 ε_{Nd} units reaching up to 2.5 ε_{Nd} units), while the Sr

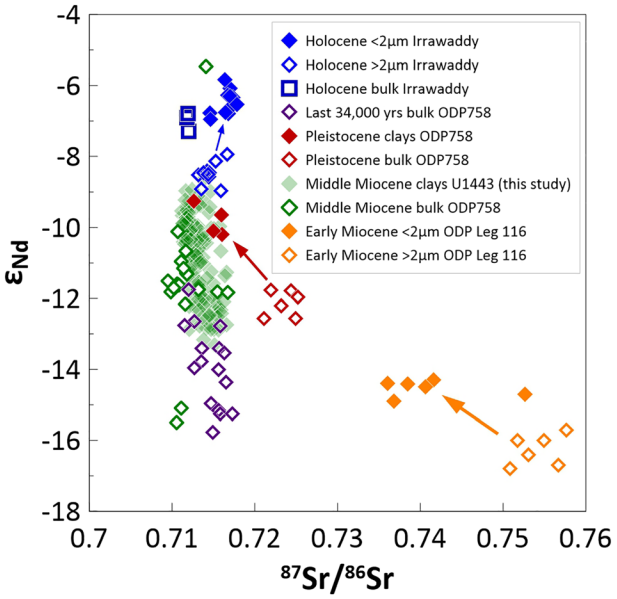

Figure 3. Grain size dependence of the radiogenic Sr and Nd isotope composition, comparing the clay (<2 µm) and bulk or >2 µm fraction of sediments from the Holocene Irrawaddy River (blue, Giosan et al., 2018, and this study), the last 34,000 years of ODP Site 758 (purple, Ahmad et al., 2005), Pleistocene of ODP Site 758 (red, Ali et al., 2021; Gourlan et al., 2010), middle Miocene of ODP Site 758 and U1443 (green, Banerjee et al., 2019 and this study), and early Miocene sediments of the distal Bengal Fan (orange, Galy et al., 1996).

isotope signatures do not differ significantly (up to 0.0057 higher values in the clays than in the silt fraction). The Pb isotope signatures are systematically more radiogenic in the silt fraction (0.1–0.2 higher $^{206}Pb/^{204}Pb$ ratios and 0.2–0.4 higher $^{208}Pb/^{204}Pb$ ratios) than in the clays.

4. Discussion

4.1. Provenance Control on the U1443 Detrital Clay Isotope Signature

Figures 4 and 5 compare the Nd-Sr and Nd-Pb isotope compositions of the U1443 clays with those of potential source areas surrounding the Bay of Bengal and the sediments sampled in the major rivers. Of the Himalayan sources, the TPB signature is almost identical to that of the IBR and is already included in the Brahmaputra sediment signatures as it is fed by the Yarlung-Tsangpo River which drains the TPB. It is therefore not considered as an independent end-member. The wide exposure of the TPB and the TSS rocks within the drainage basin of the Yarlung-Tsangpo is the main reason for the difference in isotope signatures between the Ganges, with only very sparse coverage of TSS for upper and already arid regions of its watershed, and Brahmaputra sediments and the large range of Brahmaputra compositions. Since other potential contributors of radiogenic Nd such as the Deccan Traps or the Sunda Arc (Figure 4a) are considered negligible (see discussion below), the IBR is considered the dominant contributor of sediments with radiogenic Nd and unradiogenic Sr isotope values. In contrast to the NER samples, Bengal Fan silicates with a similar age to ours clearly overlap with HHC signatures (Figure 4a; e.g., France-Lanord et al., 1993; Galy et al., 2010) and lack the IBR influence. Nevertheless, the large-scale changes are similar to the ones observed at the NER (Ali et al., 2021). Hemipelagic sediments from the Bengal Fan plot much closer to our samples (Figure 4a)

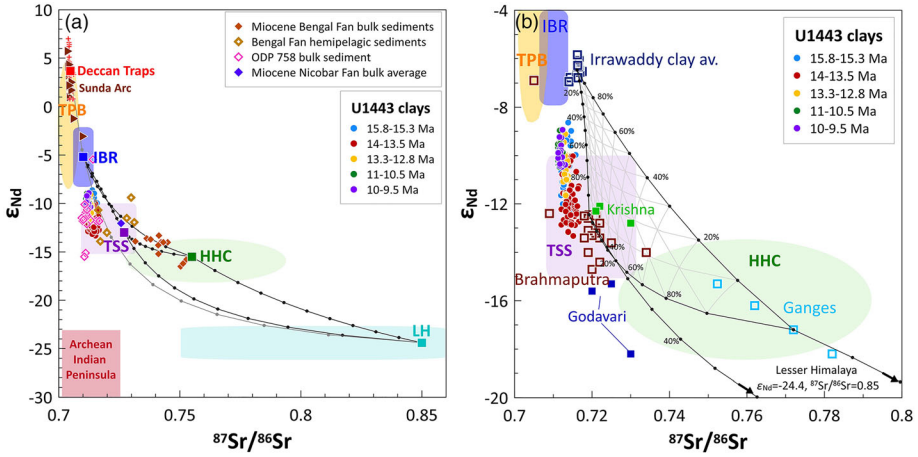

Figure 4. (a) Nd-Sr isotope composition of the clay size fraction of Site U1443 compared with published data. Miocene Bengal Fan bulk sediments (Galy et al., 2010), Bengal Fan hemipelagic sediments (Galy et al., 2010; Hein et al., 2017), the average of bulk Miocene Nicobar Fan sediments (Chen, Yan, et al., 2020), and ODP 758 bulk sediments (Banerjee et al., 2019) are plotted for comparison. Potential sources include the different Himalayan lithologies (Transhimalayan Plutonic Belt—TPB, Tethyan Sedimentary Series—TSS, High Himalayan Crystalline—HCC, and Lesser Himalayas—LH), the Indo-Burman Ranges (IBR), the Deccan Traps, the Archean Indian Peninsula, the Sunda Arc, and the rivers draining these lithologies—Irrawaddy, Ganges, and Brahmaputra (squares). References are listed in Table 1. (b) Average values of the three major rivers are used as end-members to define a mixing field. The grid was calculated according to a 10% increment of the mixture composition using the compositions listed in Table 1. U1443 clays do not plot within the mixing field but show a binary mixing trend between the Irrawaddy and the Brahmaputra Rivers.

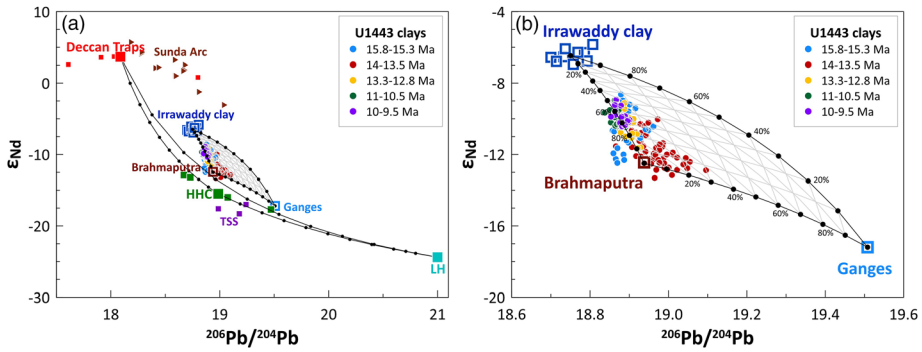

Figure 5. (a) Nd-Pb isotopic composition of U1443 clays compared to the potential sediment sources, represented by Deccan Traps, Sunda Arc, TSS, HHC, and LH average compositions as well as the Irrawaddy, Ganges, and Brahmaputra Rivers (squares, references in Table 1). (b) Expanded view of mixing field spanned by the three major rivers used as end-members. The grid was calculated according to a 10% increment of the mixture composition. The U1443 clays show a dominant contribution of Irrawaddy and Brahmaputra sources.

and were interpreted to contain significant IBR contributions (Galy et al., 2010), indicating that the NER clay radiogenic isotope compositions represent the fine-grained sediment supplied to the central basin. The overlap of our clay results with bulk detrital measurements from the same location (Figures 3 and 4a; Banerjee et al., 2019) confirms that they originate from the same sources and that grain size dependent fractionation of the isotope compositions did not have a significant impact on the reconstructed mixing relationships between the main source areas. The grain size effects are small compared to the isotopic range of source areas and therefore it is reasonable to relate the clay results to bulk sediment data.

In addition to the sediments supplied by major rivers, fine-grained mineral dust, for example, from the Thar desert, may have contributed to the U1443 clay isotopic composition. However, the calculated annual mineral dust input of ~0.3–6 g m^{-2} $year^{-1}$ to the Bay of Bengal (extrapolated to the surface area of the Bay of Bengal, the annual mineral dust input corresponds to a maximum of ~13 Mt $year^{-1}$; Srinivas & Sarin, 2013) is minor (~1%) compared to the 1,300 Mt $year^{-1}$ of sediments supplied by the Ganges, Brahmaputra and Irrawaddy Rivers (Figure 1; Milliman & Syvitski, 1992) and is therefore considered negligible. Comparison with lithogenic fluxes to sediment traps near the NER (Unger et al., 2003) suggests that the dust flux is of a similar magnitude, although recent NER sediments are clearly dominated by river derived material (e.g., Ahmad et al., 2005). During the middle Miocene, the detrital mineral flux to ODP Site 758 was elevated compared to more distal sites in the Indian Ocean which showed similar sedimentation rates (Hovan & Rea, 1992), demonstrating the persistence of enhanced continental weathering inputs to the NER.

Due to the movement of the Indian Plate, Site U1443 was located at least 800 km further south, at ~2°S during the middle Miocene. Tectonic reconstructions suggest that the location of the Indian Peninsula relative to the NER has remained the same since the Oligocene/Miocene while the NER moved closer to the Himalayas and Sundaland (Hall, 2012; Zahirovic et al., 2016). However, given that this change was relatively small between 15 and 10 Ma (Hall, 2012), plate motion most likely did not affect the source contributions of clays reaching the core location. Instead, the advancing Himalayan sediments rapidly filling basins now on land and feeding the growing Bengal and Nicobar fans likely influenced sediment accumulation on the NER (e.g., McNeill et al., 2017). The evolution of Sundaland to the east was more complex (e.g., Zahirovic et al., 2016), but the lack of volcanic detritus or any Sumatran contributions in the Nicobar Fan (Chen, Yan, et al., 2020; Pickering et al., 2020) suggests that the Sumatra magmatic arc was only a minor contributor throughout the middle Miocene. Moreover, over the last 30 Myr repeated flooding and exposure of the shelf seas around Sumatra (Zahirovic et al., 2016) should have strongly affected the sediment supply from this source, which is not consistent with the overall near stable source contributions recorded in our U1443 clays. The influence of sources from the Indian Peninsula, like the Deccan Traps or Archean terranes is also considered to be minor (Ali et al., 2021; France-Lanord et al., 1993). Deccan Trap isotope compositions of the younger and more voluminous flows display highly radiogenic Nd and unradiogenic Sr and Pb isotope compositions (Figures 4a and 5a; e.g., Lightfoot et al., 1990), while Archean Terranes are characterized by

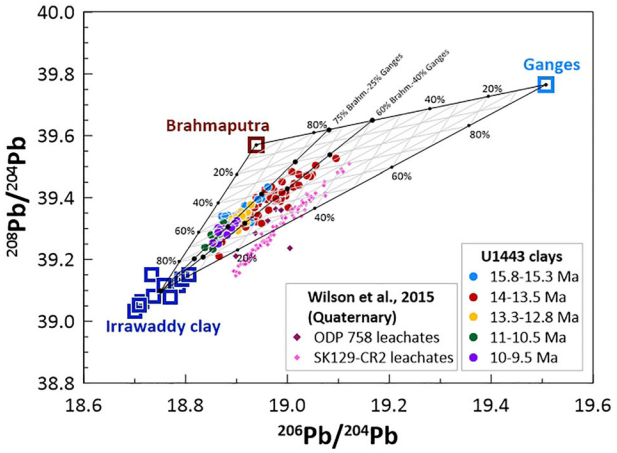

Figure 6. Pb isotopic composition of U1443 clays compared to Quaternary Indian Ocean leachate data (Wilson et al., 2015) and potential sources represented by the Irrawaddy, Ganges, and Brahmaputra Rivers (squares, references in Table 1). The three major rivers are used as end-members to span a mixing field. The grid was calculated according to a 10% increment of the mixture composition. U1443 clays plot within the mixing triangle, suggesting a mixture of source contributions. Two binary mixing lines between the Irrawaddy end-member and two Brahmaputra-Ganges mixtures show the binary mixing trend of the clays.

extremely unradiogenic ε_{Nd} signatures (Figure 4a; Kessarkar et al., 2005; Peucat et al., 1989), thus both being distinct from our clay isotope compositions. Although mixing between the Archean Indian Peninsula and the IBR end-members could produce the isotope composition of the U1443 clays, this is not reasonable given that this would require 20% to 50% contributions from Archean Indian continental sources. This is unlikely for a number of reasons. First, the Krishna and Godavari Rivers draining the Indian Peninsula reflect a combined signature of the Indian Peninsula sediments (Figure 4b), which can neither account for the more radiogenic ε_{Nd} isotope compositions nor the low $^{87}Sr/^{86}Sr$ signatures of our samples. Secondly, the supply of material from these sources by the Krishna and Godavari Rivers was likely restricted to the Indian margin due to the monsoon-induced Indian coastal current (Ali et al., 2021; Kumar et al., 2006). The east-west divide of isotope compositions in surface sediments from the Bay of Bengal (Colin et al., 1999) corroborates the fact that Peninsula river sediments are restricted to the western Bay of Bengal. Additionally, their sediment load is minor compared to that of the major rivers (Figure 1) and sediments recently deposited on the NER have a composition similar to those deposited in the Miocene (Figure 3). Consequently, we are confident that the dominant sources supplying clays to the NER are the Himalayan and IBR sources in the north and that Sundaland and Indian Peninsula sources only played a minor role.

The Pb isotope composition provides additional constraints on the sources of the clay size sediments. Figure 6 shows the U1443 clays together with typical fluvial sediments representing the catchment areas. Consistent with the Nd-Sr isotope relationships, our Pb isotope data indicate that the samples reflect a mixture of more radiogenic Himalayan sources represented by Ganges and Brahmaputra sediments and less radiogenic sources from the IBR represented by the Irrawaddy sediments. However, the estimated mixture percentages differ from those based on the Nd-Sr calculations, with an ~20% higher Irrawaddy end-member contribution.

To better constrain the different source contributions, we calculated binary mixing relationships between the most likely end-members (Table 1) and added ternary mixing grids to Figures 4b, 5, and 6. Since data for all three isotope systems exist for most of the river sediments in contrast to the major lithologies, we applied average Irrawaddy clay, and average bulk Brahmaputra and Ganges sediment isotopic signatures as mixing end-members (Figures 4–6). The Sr-Nd mixing plot shows that the U1443 clays do not fall into the field spanned by Irrawaddy, Brahmaputra and Ganges sediments (Figure 4). While ε_{Nd} values plot almost on a line between the Irrawaddy and Brahmaputra, indicating up to 60% Irrawaddy and 40–100% Brahmaputra contributions, the $^{87}Sr/^{86}Sr$ isotopic signatures are shifted toward more unradiogenic Sr values and do not overlap with any mixing trends between the three end-members. Given that contributions from seawater Sr are minimal (see Ali et al., 2021), and similar values are found for the bulk detrital data from ODP Site 758 (Figure 3) the most likely explanation for the observed shift is that the average river isotope compositions used as end-members are not well constrained. The river end-members are derived from modern day bulk river sediments (Galy & France-Lanord, 2001; Giosan et al., 2018; Singh & France-Lanord, 2002) but their isotopic compositions may have varied over the last 16 Myr. Furthermore, the spread in values of measured river sediments, especially for the Brahmaputra River, is large. Therefore, it is possible that the actual source end-members of our clays in the Miocene had less radiogenic Sr isotopic signatures than the average values applied as end-members. Additionally, Sr isotopes are known to be influenced by grain size fractionation and weathering effects (Blum & Erel, 2003; Derry & France-Lanord, 1996), which is consistent with previous work in the region that has shown detrital Sr isotopes to vary, while Nd isotopes suggest a constant source (Ali et al., 2015; Colin et al., 1999).

We thus consider the mixing relationships of the Pb-Pb and the Nd-Pb isotope system (Figures 5b and 6) more appropriate to reflect changes in the source contributions of the clays. The plots clearly show that all three end-members contributed to the NER clays. There is a clear difference between the youngest intervals (11–10.5 and 10–9.5 Ma), exhibiting little variability in source contributions (<25%) and a Ganges

Table 1
Literature Sr, Nd, and Pb Average Isotopic Compositions and Concentrations for the Major Lithologies and River Systems Used as End-Members

End-member	$^{87}Sr/^{86}Sr$	Sr (ppm)	ε_{Nd}	Nd (ppm)	$^{206}Pb/^{204}Pb$	$^{208}Pb/^{204}Pb$	References
IBR	0.71	200	−5.2	24			Awasthi et al. (2014)
TSS	0.727	229	−13	26.7			France-Lanord et al. (1993)
HHC	0.755	70	−15.5	23.6			France-Lanord et al. (1993); Singh and France-Lanord (2002)
LH	0.85	70	−24.4	40.3	21		Singh and France-Lanord (2002); Clift et al. (2002)
TPB	0.705	400	−6.5				Singh and France-Lanord (2002)
Deccan Traps	0.705	228	3.7	11	18.088		Lightfoot et al. (1990); Mahoney et al. (1982); Tripathy et al. (2011)
Archean Indian Peninsula	0.716		−25				Kessarkar et al. (2005); Peucat et al. (1989)
Sunda Arc	0.705		2.0		18.565		Gasparon and Varne (1995)
Irrawaddy	0.716	100	−6.5	50	18.751	39.098	Awasthi et al. (2014); this study
Brahmaputra	0.719	212	−12.5	35.6	18.938	39.571	Singh and France-Lanord (2002); Millot et al. (2004)
Ganges	0.772	32	−17.2	23.6	19.508	39.766	Singh and France-Lanord (2002); Millot et al. (2004)
Godavari	0.725		−16.4				Ahmad et al. (2009)
Krishna	0.724		−12.4				Ahmad et al. (2009)

contribution of <10%, and the two intervals between 15.8 and 13.5 Ma. By far the largest variability in source contributions (up to 60%) is found for the interval comprising the major cooling step at ~13.9–13.8 Ma (14–13.5 Ma). Interestingly, the samples define binary mixing trends between the Irrawaddy end-member and a rather constant Ganges-Brahmaputra mixture. The Nd-Pb isotope plot shows an almost pure Brahmaputra-Irrawaddy mixing line for all intervals except the 14–13.5 Ma interval, which shows a Ganges contribution for the Ganges-Brahmaputra end-member of 10–20%. These lower Ganges contributions agree with observations of Galy and France-Lanord (2001), who found a higher modern sediment flux from the Brahmaputra compared to the Ganges. During the Miocene, the Ganges contribution was also likely diminished by changes in the routing of the rivers as documented by differences in the composition of sediments in the Nicobar and Bengal fans (Chen, Yan, et al., 2020). In the Pb-Pb isotope space, most samples plot on the mixing line between the Irrawaddy and a 75%-Brahmaputra-25%-Ganges end-member. In agreement with the Nd-Pb isotope plot, the 14–13.5 Ma interval points to a Ganges-Brahmaputra end-member with higher Ganges contribution, in this case ~40%. Even though the percentages do not match precisely for Nd and Pb isotopes, the trend of a higher Ganges contribution during the 14–13.5 Ma interval is clear. A possible explanation for the differences may be the known influence of weathering on clay Pb isotope signatures (e.g., Erel et al., 1994; Harlavan & Erel, 2002). Across the investigated Miocene time interval, we observe a marked change in the overall balance of the sources from relatively low Irrawaddy and high Brahmaputra and Ganges contributions prior to 13.5 Ma to higher amounts (by ~20%) of Irrawaddy material delivered thereafter (Figure 2).

The radiogenic Sr, Nd, and Pb isotope compositions of the clays transported to the southern Bay of Bengal suggest that the different erosional sources have overall supplied clays during the Miocene in a remarkably consistent manner, considering the major tectonic reorganizations in the Himalayas (Ali et al., 2021). This mixture was enriched in material originating from formations with more radiogenic Nd isotope compositions (i.e., the IBR) where the monsoon rains are strongest today (Damodararao et al., 2016). Our new high-resolution data, however, reveal periods of source variability of up to 60% which were not captured by the lower-resolution study of Ali et al. (2021) (Figure 2).

4.2. Tectonic and Climatic Control on the Long-Term Radiogenic Isotope Evolution of Clays During the Miocene

On long timescales, our data document that the sources of sediments remained remarkably stable throughout the middle and early late Miocene. This is in agreement with previous Sr and Nd isotope records from the distal and central Bengal Fan spanning the last 17 Myr (France-Lanord et al., 1993) and the last 12 Myr (Galy et al., 2010), as well as the low-resolution record for the last 27 Myr from Site 758 (Ali et al., 2021). The evolution of the radiogenic isotope record between 17 and 9 Ma at Site 758 is overall consistent with our data (Figure 2). The Site 758 data are similar to the more radiogenic ε_{Nd} values and less radiogenic

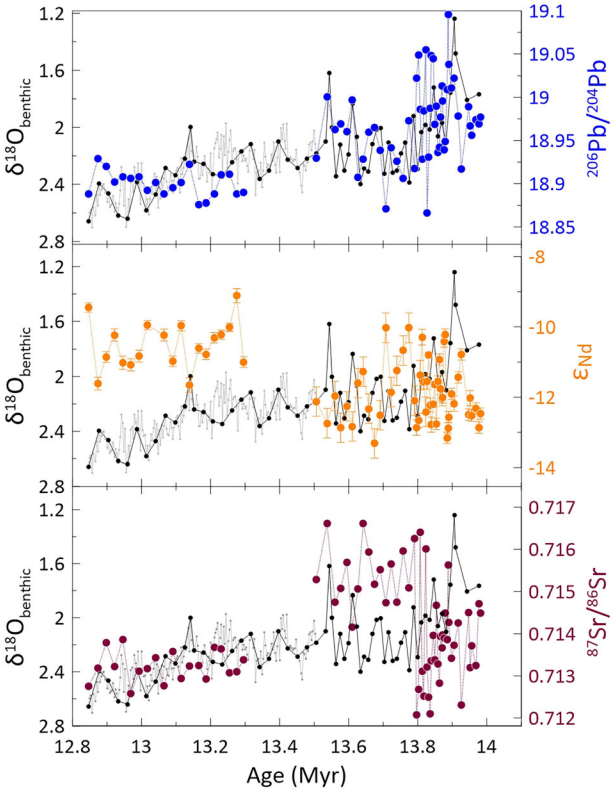

Figure 7. Radiogenic Pb, Nd and Sr isotope compositions of U1443 clays compared to the benthic $\delta^{18}O$ signal over the major middle Miocene cooling at ~13.9–13.8 Ma. The black dots and lines represent a low-resolution (~40 kyr) benthic $\delta^{18}O$ record (supporting information Table S1). The gray dots and lines in the younger part from 13.5 to 12.8 ma show the higher resolution (~5 kyr) benthic $\delta^{18}O$ record of Lübbers et al. (2019). The variability of the radiogenic isotopic composition decreases for all three isotope systems after the cooling event. The Pb isotope variations closely follow the benthic $\delta^{18}O$ curve in the older part until 13.5 Ma.

$^{206}Pb/^{204}Pb$ and $^{87}Sr/^{86}Sr$ isotope compositions of the Site U1443 clays. The higher resolution data of our study exhibit much higher variability and document increased contributions from the Himalayas (up to 20% more Ganges, up to 40% more Brahmaputra contribution). The difference between the two records may also, at least partly, originate from differences in leaching or dissolution techniques in the two studies. A weaker leaching prior to dissolution of the clay size minerals applied by Ali et al. (2021) may have left some seawater-derived authigenic signatures in the low-resolution data, while the alkaline fusion technique employed here is more likely to dissolve all refractory minerals than simple mixed acid digestion at low pressure (Bayon et al., 2009). Generally, the warmer intervals are marked by a much higher variability in all three isotope systems and by relatively higher Himalayan contributions additionally to IBR dominated samples. The colder intervals show a lower isotopic variability and contributions generally dominated by the IBR. This change occurred directly following the major global Miocene cooling, at ~13.9–13.8 Ma (Figure 7). One possible driver of this shift is therefore a change in global climate, but how could climate cooling have caused this change in radiogenic isotope variability? Warmer climates were, if similar to Holocene observations (e.g., Galy et al., 2008; Li et al., 2018), associated with a stronger land-sea surface temperature contrast, resulting in a strengthening of summer monsoon circulation and an enhanced atmospheric water vapor transport. The higher availability of water in the atmosphere during warmer intervals may then have led to increased penetration of monsoon precipitation into the high mountain areas, possibly overcoming the existing main orographic barrier (the High Himalayas), thus enabling more intense erosion in formerly arid plateau regions and higher contributions of High Himalayan (HHC) material. Climate-tectonic interactions can produce feedbacks in both directions (Clift & Webb, 2018). Since rainfall follows topography, higher erosion in highlands result from both strong precipitation and steep topography. More erosion fosters exhumation, which drives more uplift and higher topography can focus more precipitation. Therefore, the tectonic evolution of the Himalayas also needs to be included in the interpretation of the data on longer timescales.

Considering the major tectonic reorganization of the Himalayan orogenic wedge during the middle Miocene (e.g., Hodges, 2000; Vannay et al., 2004; White et al., 2002; Yin, 2006), it is remarkable that the average mixture of sediment sources deposited at Site U1443 remained consistent throughout the investigated time window. However, the marked decrease in variability in all three radiogenic isotope systems was too rapid to be related to those large tectonic changes. During the early-middle Miocene, the deformation of the wedge was dominated by the frontal accretion and mid crustal extrusion of HHC rocks between two major shear zones, the MCT to the south and the Southern Tibetan Detachment System (STDS) to the north (e.g., Hodges, 2000, and references therein). Rocks from the MCT hanging wall, comprising HHC and TSS, were exhumed and eroded (Vannay et al., 2004; White et al., 2002). Thereafter, during the middle Miocene, the thrusting propagated south from the MCT, shifting the exhumation to the Lesser Himalayan (LH) units, while the exhumation of the HHC and TSS slowed down (Colleps et al., 2019; Najman et al., 2009). Still, High Himalayan lithologies covered large parts of the Himalayas. The LH units, covering the Indian craton, underthrusted the Himalayan wedge, accreted and formed the LH-duplex. These processes shifted the main orographic barrier southward from within the Lhasa Block to its current position in the High Himalayas (Tremblay et al., 2015). This shift likely had a large impact on which rocks were exposed to erosion. The exact timing of the tectonic changes is difficult to constrain, but most studies agree on a peak time of rapid exhumation of the HHC, TSS, and TPB at ~17–16 Ma (Carrapa et al., 2014; Colleps et al., 2018; Tremblay et al., 2015),

while the timing for the slowdown of exhumation varies between ~16 Ma (Najman et al., 2009) and ~10 Ma (Tremblay et al., 2015). One way to explain those different ages is the locally restricted sampling of these studies, whereas our record provides an integrated signal of the different sediment sources in the catchment areas of the rivers. Before this tectonic reorganization, a mixture of TSS and HHC rocks were dominantly eroded. The two intervals prior to 13.5 Ma include higher $^{87}Sr/^{86}Sr$ and lower ε_{Nd} values than the subsequent intervals, typical for more High Himalayan-influenced sources. The main orographic barrier was positioned further north, which would have enabled high erosion rates across the Indus-Tsangpo suture zone and the southern Tibetan Plateau and a steeper and very erosive drainage network across the Himalayas (Tremblay et al., 2015; White et al., 2002). Moreover, under these conditions, Tremblay et al. (2015) also expect a wetter precipitation regime on the southern Tibetan Plateau, which drove large-scale erosional exhumation. This is in agreement with thermochronological data of Carrapa et al. (2014) that document the removal of large volumes of rock from the suture zone within a few million years. This can only be accomplished by sufficient precipitation, efficient river incision and enhanced sediment transport due to an intensified SAM across these internal parts of the mountain belt during and around the MCO.

The tectonic reorganization, including the southward propagation of the thrusting and the accompanied southward shift of the orographic barrier, as well as the decrease in High Himalayan exhumation, restricted the erosion of Himalayan source rocks. The reorganization of the drainage system most likely resulted in a much smoother channel slope and thus in decreasing stream power. Moreover, due to the southward shift of the orographic barrier, the precipitation no longer reached the interior of the southern Tibetan plateau and aridity increased. The decrease in stream power and the increase in aridity probably resulted in the shutdown of erosion in Southern Tibet, which Tremblay et al. (2015) considered to have happened at the latest around 10 Ma. The shutdown of intense erosion is documented by the low variability and the decrease in Himalayan source contributions in the U1443 record after 13.5 Ma, thus considerably earlier than the estimated age of Tremblay et al. (2015). As mentioned before, this could be due to the integrated sediment signal of Site U1443 in contrast to the local study of Tremblay et al. (2015). After the erosion of the MCT hanging wall units, erosion of LH units, as part of the exhuming LH-duplex after the reorganization, would be expected (Colleps et al., 2018). However, there is a complete lack of LH signatures (Figure 4, $\varepsilon_{Nd} \approx -24.4$, $^{87}Sr/^{86}Sr \approx 0.85$; Singh & France-Lanord, 2002) in our record, as well as in Miocene Bengal Fan records (France-Lanord et al., 1993; Galy et al., 1996), implying no extensive weathering and supply of these lithologies as clays. A possible explanation for the missing signal of the LH is that LH units are much more dominant in the central Himalayas drained by the Ganges, while they are hardly exposed in the eastern part (Figure 1), which is the major watershed of the Brahmaputra. Our provenance estimates clearly indicate a dominance of Brahmaputra over Ganges contributions for the Himalayan component, which can at least partly explain the absence of LH influence across the east. The continued supply of HHC, TSS and TPB derived material following the mid-Miocene shutdown of strong erosion of these terrains suggests that these sources were weathered to form clay minerals in deposits such as those forming the IBR.

The decrease in variability of the radiogenic isotope signatures at 13.5 Ma closely followed the Miocene cooling (major cooling step at ~13.9–13.8 Ma) documented by the benthic $\delta^{18}O$ record and occurred abruptly within only ~200 kyr (Figure 7). This geologically short time period argues for a coupling of climate and erosion and implies that tectonics were not the main driver of this change. Both, vigorous erosion accompanied by rapid sediment transport and deposition of organic material with clastic sediments across the mega fans, as well as chemical weathering of Himalayan material, may have contributed to CO_2 drawdown and thus to the global cooling throughout the Cenozoic. Simultaneously, the cooling climate, whether supported by Himalayan erosion or not, likely had a huge impact on precipitation patterns. While strong precipitation appears to have reached deeper into the High Himalayas during the warm period around the MCO, its geographic extent was likely decreased with the cooling and focused on the frontal domain of Himalayan orogenic belt. The orographic barrier of the High Himalaya during cooler climate became active in preventing precipitation from reaching the high elevations and distal (from the moisture source) parts (including HHC and TSS) of the southern Tibetan Plateau margin. In turn, without strong erosion, exhumation would be diminished, which is supported by the slowdown in exhumation and erosion of the High Himalayas, the Tethyan Himalayas, the suture zone region and the southern Lhasa Block sometime between 17 and 10 Ma (Najman et al., 2009; Tremblay et al., 2015; White et al., 2002). The increase in sediment flux to the NER following the middle Miocene cooling, as inferred from the study by Hovan and Rea (1992; recalculated

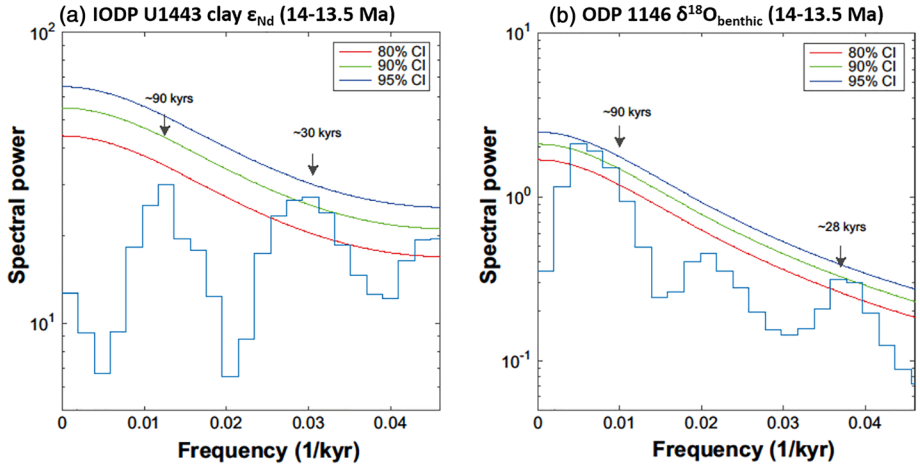

Figure 8. REDFIT spectral analysis of (a) Nd isotope compositions of the U1443 clay samples, and (b) benthic $\delta^{18}O$ time series of ODP Site 1146 (Holbourn et al., 2010) for the interval spanning from 14 to 13.5 Ma. The values of the oversample and segments applied were two and three, respectively.

by Ali et al., 2021; Figure 2), seems contradictory to the decrease in High Himalayan erosion. However, the increase in sediment flux might only reflect the progradation of the accumulating Bengal Fan, with suspension transport reaching the top of the NER (Ali et al., 2021). This in turn can be questioned due to the evidence of simultaneous increases in sedimentation at nearby drill sites on the Bengal Fan (Ali et al., 2021). Furthermore, the climatic and/or tectonic changes did not necessarily lead to a general decrease in erosion within the watersheds supplying the Bay of Bengal. Instead, they altered the precipitation pattern and the locus of maximum erosion to more frontal and southern domains of the Himalayas as well as to the present-day LH, which was still mainly covered by High Himalayan thrust nappes during the middle and late Miocene. The focus of monsoonal rains shifted to lower altitudes along the southern Himalayan front, as seen today (Bookhagen et al., 2006) and to the IBR, hence eroding and weathering more material with less radiogenic Sr and Pb and more radiogenic Nd signatures, as reflected by our record. Therefore, the increased sediment delivery to the fans and NER during the Miocene could simply be the result of the shorter transport distance for the sediments derived from the frontal domains of the Himalayas compared to material traveling the distance across the entire orogenic belt. The increase of the primary clay mineral illite during the cooling suggests an increase in physical erosion, which may have been associated with increased aridity in the colder climate (Ali et al., 2021). This also hints at the focus of precipitation on the IBR after the cooling, since the Irrawaddy River does not have an extensive floodplain, as opposed to the Indo-Gangetic plain (Joussain et al., 2016; Li et al., 2018), an environment in which intense chemical weathering producing secondary clay minerals takes place. Ali et al. (2021) interpreted the increase of the primary clay mineral supply accompanied by only subtle changes in the mixture of the source rocks being weathered as resulting from a shift in the weathering regime. This shift during the middle Miocene global cooling likely resulted from the development of the dry NE winter monsoon season (Ali et al., 2021), similar to what had been inferred for the late Miocene in East Asia (Holbourn et al., 2018).

4.3. Climatic Control on Source Contributions and the Weathering Regime of the Bay of Bengal Catchment Areas Causing Fluctuations of Radiogenic Isotopes on Orbital Timescales

The reversible nature of the short-term fluctuations means that they cannot have been caused by tectonics, given that major tectonic reorganizations only occur on longer (Myr) timescales and are generally unidirectional. The changes in isotopic compositions within the individual Miocene time intervals occurred on orbital timescales of a few to tens of thousands of years (Figures 2 and 7).

Spectral analyses of the high-resolution ε_{Nd} data obtained between 14 and 13.5 Ma with a much higher average sampling resolution than ~10 kyr and consequently smaller aliasing errors, document a significant ~30 kyr cyclicity with additional contributions of the ~100 kyr eccentricity (Figure 8; for more details, see

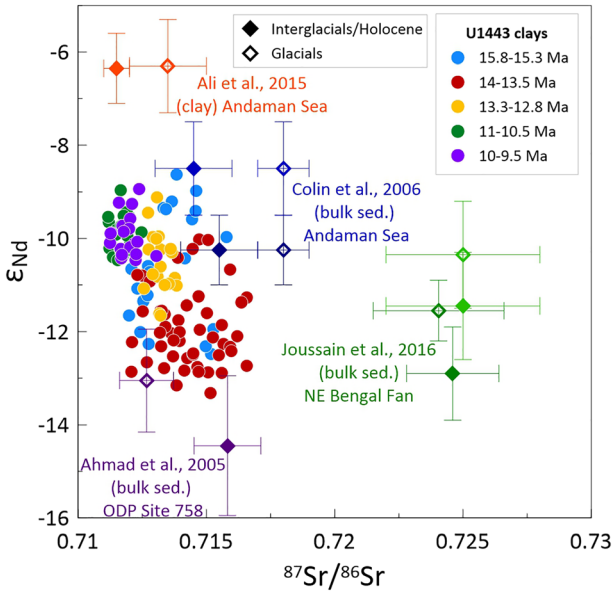

Figure 9. The ε_{Nd} versus $^{87}Sr/^{86}Sr$ cross plot of U1443 detrital clay data for all five intervals together with average glacial versus interglacial values from the literature (Ahmad et al., 2005; Ali et al., 2015; Colin et al., 2006; Joussain et al., 2016). There are two glacial/interglacial average values for the Colin et al. (2006) and Joussain et al. (2016) studies to account for two different sediment core locations.

also supporting information). Although not as pronounced, an ~30 kyr cyclicity (>80% Confidence Interval, CI) is also apparent in the Pb isotope data (not shown) but we did not find a similar periodicity in the $^{87}Sr/^{86}Sr$ data. This ~30 kyr periodicity is most likely a heterodyne produced by interaction of the three major orbital cycles and is commonly observed in late Quaternary paleoceanographic and paleoclimatic records of the South (e.g., Chen, Xu, et al., 2020; Gebregiorgis et al., 2018) and East Asian monsoon domains (e.g., Beaufort et al., 2003; Clemens et al., 2018; Sun et al., 2010). An ~ 30 kyr periodicity was also observed in planktonic oxygen isotopes reflecting surface ocean conditions in the South China Sea during the middle Miocene (Holbourn et al., 2010). In the late Quaternary, this heterodyne reflects the non-linearity of the monsoon strength versus external insolation relationship and the fact that this is the strongest periodicity found in the middle Miocene data suggests this may reflect the strongest monsoon variations resulting in fluctuations in clay provenance. A strong precession signal has been observed in clay mineralogy variations of late Quaternary sediments from the Bay of Bengal (e.g., Colin et al., 1999, 2006) and although the resolution of the mid-Miocene clay isotope data is generally not sufficient to resolve precession, there is a hint of a signal (>80% CL) in the Nd isotope data (Figure 8). Although only possible for the interval with the highest resolution data, these analyses suggest that the high frequency variability in the mixture of clay sources was related to changes in monsoon strength during the middle Miocene.

Since no other orbital-scale resolution Miocene records for radiogenic isotopes exist, we compare our record to Late Quaternary glacial-interglacial records that exhibit changes of radiogenic isotopic compositions of similar range and on comparable timescales to ours (Figures 6 and 9). The Pb isotope record of the authigenic sediment fraction representing dissolved deep Indian Ocean water signatures from the NER and the Central Indian Ocean of the last 250 kyr of Wilson et al. (2015) shows a range of Pb isotopic signatures very close to the ones in our detrital record (Figure 6). The variations in Pb isotopes show enhancement of Himalayan contributions by a factor of two to three during interglacial periods. The shifts in source contributions were attributed to changes in regional weathering intensity (Wilson et al., 2015). Cyclic changes in radiogenic isotopic compositions of the bulk silicate fraction from turbiditic Bengal Fan sediments during the last glacial and transition to the Holocene (Joussain et al., 2016; Li et al., 2018) were attributed to sea level changes and to changing surface currents responding to monsoon intensity and resulting changes in detrital supply. Moreover, a stronger summer monsoon during warmer climates (e.g., Galy et al., 2008; Li et al., 2018) may influence the source contributions not only on long timescales as discussed above but also on short timescales. Increased precipitation over the high mountain areas likely provided higher contributions of High Himalayan material during warmer climatic episodes.

It has been suggested that the strengthening of surface currents in the Bay of Bengal associated with monsoon intensification controlled the deposition of detrital inputs (Ahmad et al., 2005; Joussain et al., 2016; Li et al., 2018). Enhanced IBR source dominance within the short-term fluctuations may thus be explained by a weakening of the summer monsoon and a stronger winter (NE) monsoon. This may have become particularly important following intensification of the winter monsoon during the major cooling at ~13.9–13.8 Ma (Ali et al., 2021). Stronger NE winds likely started to drive counterclockwise currents within the Bay of Bengal, increasing the transport of sediment from the Irrawaddy River to Site U1443 (Rao et al., 2005). Such an interpretation was also favored by Ahmad et al. (2005), who recorded pulses of less radiogenic Sr (−0.003 in $^{87}Sr/^{86}Sr$) and more radiogenic detrital Nd isotope values (+1.4 ε_{Nd} units) associated with higher silt abundances during Heinrich intervals linked to an enhanced NE monsoon. Joussain et al. (2016) and Li et al. (2018) also found decreases in ε_{Nd} values (~2 ε_{Nd} units) in interglacials and the Holocene, respectively, compared to glacial periods, which, among other factors, were attributed to changing surface currents. An increase in the transport of Himalayan material to the NER during periods of a stronger summer monsoon and associated strengthened currents coming from the SW is not quite so obvious.

However, it is plausible that during enhanced summer (SW) monsoon, the mixing of sediments within the Bay of Bengal was stronger, with clockwise surface currents picking up larger amounts of Himalayan material and transporting it to the NER than during times of dominant winter monsoon. If the same mechanisms apply to the clay distribution, a doubling of Himalayan input during times of enhanced summer monsoon can account for most of the variations in our clay record. However, the glacial-interglacial changes may be mainly attributable to differences in grain size contributions. Higher silt supply during glacials does not necessarily imply higher clay supply. Clays stay in suspension until they are removed by ballasting, and by the time they would get to the NER, the clay's radiogenic isotope signal should be well mixed. Therefore, transport processes should only play a minor role in influencing our clay isotope record.

In addition to changing surface currents, Joussain et al. (2016) and Li et al. (2018) also attributed changes in sediment contribution to the sea level rise and fall between glacials and interglacials. The presence of eccentricity cycles in the record (Figure 8) points to a sea level influence on the Nd isotope composition, even though this was probably not the primary driver. The middle Miocene sea level was likely ~55 to 75 m higher than today (e.g., John et al., 2004; Miller et al., 2005, 2020) and differed even more from Later Quaternary glacial sea level. Therefore, we cannot simply transfer the glacial-interglacial sea level conclusions to the radiogenic isotope excursions apparent in our Miocene record. Nevertheless, sea level variations of ~20 m (Miller et al., 2005, 2020) between warmer and colder episodes of the Miocene would have significantly influenced the extent of the floodplains, the areas where the majority of the secondary clay minerals (which clearly dominate over the primary clay minerals, Figure 2) formed and where sediment was stored. Hence, sea level changes might not have significantly influenced transport pathways in the Miocene, which, as discussed above, should not have a major influence on the clay isotope signatures, but it would have controlled the storage and chemical weathering of the sediments and, consequently, which sediments eventually were supplied to the NER.

The processes discussed above can explain the range and changes of the radiogenic isotope compositions of the U1443 clays. This is primarily true for Nd and Pb isotope variability, which almost exclusively originates from mixing of the source end-members. The fact that ε_{Nd} and $^{87}Sr/^{86}Sr$ do not correlate well within the individual time intervals investigated (Figure 9) and that no orbital cycles are present in the Sr isotope record, however, indicates an additional incongruent weathering influence on the Sr isotopic signatures of the clays. The incongruent release of particular mineral phases most likely adds some “noise” to the signal originating from mixing of the sources. Moreover, the sea level fluctuations discussed above, and the accompanied floodplain changes, would have significantly affected the extent of chemical weathering of the sediments. Comparison to results of previous studies that interpreted the Sr isotope variability to be related to weathering regime changes, suggests that incongruent weathering contributed up to ~0.003 of the $^{87}Sr/^{86}Sr$ signature of U1443 clays (Blum & Erel, 1995).

Overall, the spectral analyses of the highest resolution data hint to the fluctuations in clay source being forced by strong variations in monsoon strength while the reduction in variability may have resulted from climate and sea level changes influencing the weathering of foreland sediments.

5. Conclusions

We present the first orbital-scale resolution Miocene records of the radiogenic Sr, Nd, and Pb isotope compositions of detrital clays from IODP Site U1443 in the southern Bay of Bengal. Our records focus on key intervals of the middle Miocene and allow us to distinguish tectonic and climatic forcing of monsoon intensity, weathering regime, and erosion intensity of the watersheds feeding into the Bay of Bengal. The clay radiogenic isotope signatures indicate that throughout the Miocene intervals, the source of the clays originated from a mixture of the High Himalayan Crystalline, the Tethyan Sedimentary Series, and Indo-Burman Ranges. This is remarkable considering the major tectonic orogenic reorganization that took place in the Himalayas during the Miocene. A marked and sudden decrease in average values and variability of the isotope signatures occurred between 13.5 and 13.3 Ma after the middle Miocene global cooling step. While the warmer intervals prior to 13.5 Ma were marked by a much higher variability in the compositions of all three isotope systems and by increased Himalayan contributions, inferred from up to 40% of the detrital material having been supplied by the Ganges River, the colder intervals were characterized by lower isotopic variability and increased relative contributions from the Indo-Burman-Ranges. This change in variability

coincided with the tectonic reorganization of thrusting, shifting the main orographic barrier to the south and slowing down exhumation of extended internal regions of the High Himalayas, Tethyan Himalayas and suture zone regions to the north. While tectonic reorganization likely had some background influence, the relatively short period of 200 kyr, during which most of the change happened, argues for global climate cooling having been the primary driver for the decrease in radiogenic isotope variability at Site U1443 due to the associated impact on precipitation patterns causing a restriction of the supply of High Himalayan erosion products.

The fluctuations of the isotope signatures on orbital timescales were mainly triggered by changes in the balance of source contributions and were climatically driven. Since the grain size was confined to the clay fraction, transport related effects are considered minor. The major control on those short-term fluctuations were likely shifts of weathering regimes on land, influenced by changes of the locus of peak monsoon precipitation between higher and lower elevations. This is supported by the presence of a significant 30 kyr periodicity in the Nd isotope record, a heterodyne typically associated with monsoon variability, as well as 100 kyr eccentricity cycles in the record, which may reflect changes in sea level affecting the spatial variation of floodplain extent.

Data Availability Statement

Data files are archived at the Data Publisher for Earth and Environmental Science (https://doi.org/10.1594/PANGAEA.922759).

Acknowledgments

Two anonymous reviewers and Editor Matthew Huber are acknowledged for their highly constructive and helpful comments which significantly improved the manuscript. This research used samples and data provided by the International Ocean Discovery Program and was funded by the German Research Foundation (DFG) (grants HA 5751/6-1 and HA 5751/6-2, KU 649/36-1, and TH 1317-8 and TH 1317-9). We thank Jutta Heinze for her help in the laboratory and Marcus Gutjahr for his assistance with measuring Pb and Nd isotope ratios on the Thermo Scientific Neptune Plus MC-ICP-MS.

Open access funding enabled and organized by Projekt DEAL.

References

Ahmad, S. M., Anil Babu, G., Padmakumari, V. M., Dayal, A. M., Sukhija, B. S., & Nagabhushanam, P. (2005). Sr, Nd isotopic evidence of terrigenous flux variations in the Bay of Bengal: Implications of monsoons during the last ~34,000 years. *Geophysical Research Letters*, *32*, L22711. https://doi.org/10.1029/2005GL024519

Ahmad, S. M., Padmakumari, V., & Babu, G. A. (2009). Strontium and neodymium isotopic compositions in sediments from Godavari, Krishna and Pennar Rivers. *Current Science*, 1766–1769.

Ali, S., Hathorne, E. C., & Frank, M. (2021). Persistent provenance of South Asian Monsoon induced silicate weathering over the past 27 million years. *Paleoceanography and Paleoclimatology*, *36*, e2020PA003909. https://doi.org/10.1029/2020PA003909

Ali, S., Hathorne, E. C., Frank, M., Gebregiorgis, D., Stattegger, K., Sumpf, R., et al. (2015). South Asian monsoon history over the past 60 kyr recorded by radiogenic isotopes and clay mineral assemblages in the Andaman Sea. *Geochemistry, Geophysics, Geosystems*, *16*, 505–521. https://doi.org/10.1002/2014GC005586

Allen, M. B., & Armstrong, H. A. (2012). Reconciling the Intertropical Convergence Zone, Himalayan/Tibetan tectonics, and the onset of the Asian monsoon system. *Journal of Asian Earth Sciences*, *44*, 36–47.

Awasthi, N., Ray, J. S., Singh, A. K., Band, S. T., & Rai, V. K. (2014). Provenance of the Late Quaternary sediments in the Andaman Sea: Implications for monsoon variability and ocean circulation. *Geochemistry, Geophysics, Geosystems*, *15*, 3890–3906. https://doi.org/10.1002/2014GC005462

Baker, J., Peate, D., Waight, T., & Meyzen, C. (2004). Pb isotopic analysis of standards and samples using a ^{207}Pb–^{204}Pb double spike and thallium to correct for mass bias with a double-focusing MC-ICP-MS. *Chemical Geology*, *211*(3–4), 275–303.

Banerjee, B., Masood Ahmad, S., Babu, E. V. S. S. K., Padmakumari, V. M., Kumar Beja, S., Satyanarayanan, M., & Keshav Krishna, A. (2019). Geochemistry and isotopic study of southern Bay of Bengal sediments: Implications for provenance and paleoenvironment during the middle Miocene. *Palaeogeography, Palaeoclimatology, Palaeoecology*, *514*, 156–167.

Bayon, G., Barrat, J. A., Etoubleau, J., Benoit, M., Bollinger, C., & Révillon, S. (2009). Determination of rare earth elements, Sc, Y, Zr, Ba, Hf and Th in geological samples by ICP-MS after Tm addition and alkaline fusion. *Geostandards and Geoanalytical Research*, *33*(1), 51–62.

Beaufort, L. d., de Garidel-Thoron, T., Linsley, B., Oppo, D., & Buchet, N. (2003). Biomass burning and oceanic primary production estimates in the Sulu Sea area over the last 380 kyr and the East Asian monsoon dynamics. *Marine Geology*, *201*(1–3), 53–65.

Belshaw, N., Freedman, P., O'Nions, R., Frank, M., & Guo, Y. (1998). A new variable dispersion double-focusing plasma mass spectrometer with performance illustrated for Pb isotopes. *International Journal of Mass Spectrometry*, *181*(1–3), 51–58.

Blum, J. D., & Erel, Y. (1995). A silicate weathering mechanism linking increases in marine ^{87}Sr/^{86}Sr with global glaciation. *Nature*, *373*(6513), 415–418.

Blum, J. D., & Erel, Y. (2003). Radiogenic isotopes in weathering and hydrology. *Treatise on Geochemistry*, *5*. https://doi.org/10.1016/B0-08-043751-6/05082-9

Blum, J. D., Erel, Y., & Brown, K. (1993). ^{87}Sr/^{86}Sr ratios of Sierra Nevada stream waters: Implications for relative mineral weathering rates. *Geochimica et Cosmochimica Acta*, *57*(21–22), 5019–5025.

Bolton, C. T., Chang, L., Clemens, S. C., Kodama, K., Ikehara, M., Medina-Elizalde, M., et al. (2013). A 500,000 year record of Indian summer monsoon dynamics recorded by eastern equatorial Indian Ocean upper water-column structure. *Quaternary Science Reviews*, *77*, 167–180. https://doi.org/10.1016/j.quascirev.2013.07.031

Bookhagen, B., Fleitmann, D., Nishiizumi, K., Strecker, M. R., & Thiede, R. C. (2006). Holocene monsoonal dynamics and fluvial terrace formation in the northwest Himalaya, India. *Geology*, *34*(7), 601.

Bouquillon, A., France-Lanord, C., Michard, A., & Tiercelin, J.-J. (1990). Sedimentology and isotopic chemistry of the Bengal Fan sediments: The denudation of the Himalaya. *Proceeding of the Ocean Drilling Program, Scientific Results*, *116*, 43–58.

Burchfiel, B. C., Zhiliang, C., Hodges, K. V., Yuping, L., Royden, L. H., & Changrong, D. (1992). The South Tibetan detachment system, Himalayan orogen: Extension contemporaneous with and parallel to shortening in a collisional mountain belt. *Geological Society of America*. https://doi.org/10.1130/SPE269-p1

Carrapa, B., Orme, D. A., DeCelles, P. G., Kapp, P., Cosca, M. A., & Waldrip, R. (2014). Miocene burial and exhumation of the India-Asia collision zone in southern Tibet: Response to slab dynamics and erosion. *Geology*, *42*(5), 443–446.

Catlos, E. J., Dubey, C. S., Harrison, T. M., & Edwards, M. A. (2004). Late Miocene movement within the Himalayan Main Central Thrust shear zone, Sikkim, north-east India. *Journal of Metamorphic Geology*, *22*(3), 207–226.

Chen, H., Xu, Z., Lim, D., Clift, P. D., Chang, F., Li, T., et al. (2020). Geochemical records of the provenance and silicate weathering/erosion from the eastern Arabian Sea and their responses to the Indian summer monsoon since the Mid-Pleistocene. *Paleoceanography and Paleoclimatology*, *35*, e2019PA003732. https://doi.org/10.1029/2019PA003732

Chen, W.-H., Yan, Y., Clift, P. D., Carter, A., Huang, C.-Y., Pickering, K. T., et al. (2020). Drainage evolution and exhumation history of the eastern Himalaya: Insights from the Nicobar Fan, northeastern Indian Ocean. *Earth and Planetary Science Letters*, *548*, 116472. https://doi.org/10.1016/j.epsl.2020.116472

Clemens, S., Holbourn, A., Kubota, Y., Lee, K., Liu, Z., Chen, G., et al. (2018). Precession-band variance missing from East Asian monsoon runoff. *Nature Communications*, *9*(1), 1–12.

Clemens, S. C., Kuhnt, W., LeVay, L. J., Anand, P., Ando, T., Bartol, M., et al. (2016). Site U1443. In S. C. Clemens, W. Kuhnt, L. J. LeVay, & the Expedition 353 Scientists (Eds.), *Indian Monsoon Rainfall*. *Proceedings of the International Ocean Discovery Program, 353*. College Station, TX: International Ocean Discovery Program. https://doi.org/10.14379/iodp.proc.353.103.2016

Clift, P. D., Hodges, K. V., Heslop, D., Hannigan, R., Van Long, H., & Calves, G. (2008). Correlation of Himalayan exhumation rates and Asian monsoon intensity. *Nature Geoscience*, *1*(12), 875–880.

Clift, P. D., Lee, J. I., Hildebrand, P., Shimizu, N., Layne, G. D., Blusztajn, J., et al. (2002). Nd and Pb isotope variability in the Indus River System: Implications for sediment provenance and crustal heterogeneity in the Western Himalaya. *Earth and Planetary Science Letters*, *200*(1–2), 91–106. https://doi.org/10.1016/S0012-821X(02)00620-9

Clift, P. D., & Webb, A. A. G. (2018). A history of the Asian monsoon and its interactions with solid Earth tectonics in Cenozoic South Asia. *Geological Society, London, Special Publications*, *483*(1), 631–652.

Cohen, A. S., O'Nions, R. K., Siegenthaler, R., & Griffin, W. L. (1988). Chronology of the pressure-temperature history recorded by a granulite terrain. *Contributions to Mineralogy and Petrology*, *98*(3), 303–311.

Colin, C., Turpin, L., Bertaux, J., Desprairies, A., & Kissel, C. (1999). Erosional history of the Himalayan and Burman ranges during the last two glacial-interglacial cycles. *Earth and Planetary Science Letters*, *171*, 647–660.

Colin, C., Turpin, L., Blamart, D., Frank, N., Kissel, C., & Duchamp, S. (2006). Evolution of weathering patterns in the Indo-Burman Ranges over the last 280 kyr: Effects of sediment provenance on 87Sr/86Sr ratios tracer. *Geochemistry, Geophysics, Geosystems*, *7*, Q03007. https://doi.org/10.1029/2005GC000962

Colleps, C. L., McKenzie, N. R., Stockli, D. F., Hughes, N. C., Singh, B. P., Webb, A. A. G., et al. (2018). Zircon (U-Th)/He thermochronometric constraints on Himalayan Thrust Belt Exhumation, bedrock weathering, and Cenozoic seawater chemistry. *Geochemistry, Geophysics, Geosystems*, *19*, 257–271. https://doi.org/10.1002/2017GC007191

Colleps, C. L., Stockli, D. F., McKenzie, N. R., Webb, A. A. G., & Horton, B. K. (2019). Neogene kinematic evolution and exhumation of the NW India Himalaya: Zircon geo- and thermochronometric insights from the fold-thrust belt and foreland basin. *Tectonics*, *38*, 2059–2086. https://doi.org/10.1029/2018TC005304

Curray, J. R., Emmel, F. J., & Moore, D. G. (2003). The Bengal Fan: Morphology, geometry, stratigraphy, history and processes. *Marine and Petroleum Geology*, *19*(10), 1191–1223.

Damodararao, K., Singh, S. K., Rai, V. K., Ramaswamy, V., & Rao, P. S. (2016). Lithology, monsoon and sea-surface current control on provenance, dispersal and deposition of sediments over the Andaman continental shelf. *Frontiers in Marine Science*, *3*. https://doi.org/10.3389/fmars.2016.00118

Deng, T., Wang, X., Wu, F., Wang, Y., Li, Q., Wang, S., & Hou, S. (2019). Review: Implications of vertebrate fossils for paleo-elevations of the Tibetan Plateau. *Global and Planetary Change*, *174*, 58–69.

Derry, L. A., & France-Lanord, C. (1996). Neogene Himalayan weathering history and river 87Sr, 86Sr: Impact on the marine Sr record. *Earth and Planetary Science Letters*, *142*, 59–74.

Erel, Y., Harlavan, Y., & Blum, J. D. (1994). Lead isotope systematics of granitoid weathering. *Geochimica et Cosmochimica Acta*, *58*(23), 5299–5306.

Foster, G. L., Lear, C. H., & Rae, J. W. B. (2012). The evolution of pCO_2, ice volume and climate during the middle Miocene. *Earth and Planetary Science Letters*, *341–344*, 243–254.

France-Lanord, C., Derry, L., & Michard, A. (1993). Evolution of the Himalaya since Miocene time: Isotopic and sedimentological evidence from the Bengal Fan. *Geological Society, London, Special Publications*, *74*(1), 603–621.

France-Lanord, C., & Derry, L. A. (1997). Organic carbon burial forcing of the carbon cycle from Himalayan erosion. *Nature*, *390*(6655), 65–67.

France-Lanord, C., & Le Fort, P. (1988). Crustal melting and granite genesis during the Himalayan collision orogenesis. *Transactions of the Royal Society of Edinburgh: Earth Sciences*, *79*(2–3), 183–195.

Galer, S. J. G., & O'Nions, R. K. (1989). Chemical and isotopic studies of ultramafic inclusions from the San Carlos volcanic field, Arizona: A bearing on their petrogenesis. *Journal of Petrology*, *30*, 1033–1064.

Galy, A., & France-Lanord, C. (2001). Higher erosion rates in the Himalaya: Geochemical constraints on riverine fluxes. *Geology*, *29*(1), 23.

Galy, A., France-Lanord, C., & Derry, L. A. (1996). The Late Oligocene-Early Miocene Himalayan belt constraints deduced from isotopic compositions of Early Miocene turbidites in the Bengal Fan. *Tectonophysics*, *260*, 109–118.

Galy, V., France-Lanord, C., Beyssac, O., Faure, P., Kudrass, H., & Palhol, F. (2007). Efficient organic carbon burial in the Bengal fan sustained by the Himalayan erosional system. *Nature*, *450*(7168), 407–410.

Galy, V., France-Lanord, C., Peucker-Ehrenbrink, B., & Huyghe, P. (2010). Sr–Nd–Os evidence for a stable erosion regime in the Himalaya during the past 12 Myr. *Earth and Planetary Science Letters*, *290*, 474–480.

Galy, V., François, L., France-Lanord, C., Faure, P., Kudrass, H., Palhol, F., & Singh, S. K. (2008). C4 plants decline in the Himalayan basin since the Last Glacial Maximum. *Quaternary Science Reviews*, *27*(13–14), 1396–1409.

Gansser, A. (1964). *Geology of the Himalayas*. London: Interscience.

Gasparon, M., & Varne, R. (1995). Sumatran granitoids and their relationship to Southeast Asian terranes. *Tectonophysics*, *251*, 277–299.

Gebregiorgis, D., Hathorne, E. C., Giosan, L., Clemens, S., Nürnberg, D., & Frank, M. (2018). Southern Hemisphere forcing of South Asian monsoon precipitation over the past ~1 million years. *Nature Communications*, *9*(1).

Giosan, L., Naing, T., Min Tun, M., Clift, P. D., Filip, F., Constantinescu, S., et al. (2018). On the Holocene evolution of the Ayeyawady megadelta. *Earth Surface Dynamics*, *6*(2), 451–466. https://doi.org/10.5194/esurf-6-451-2018

Gourlan, A. T., Meynadier, L., Allègre, C. J., Tapponnier, P., Birck, J.-L., & Joron, J.-L. (2010). Northern Hemisphere climate control of the Bengali rivers discharge during the past 4 Ma. *Quaternary Science Reviews*, *29*(19–20), 2484–2498.
Gutjahr, M., Frank, M., Stirling, C. H., Klemm, V., van de Flierdt, T., & Halliday, A. N. (2007). Reliable extraction of a deepwater trace metal isotope signal from Fe–Mn oxyhydroxide coatings of marine sediments. *Chemical Geology*, *242*(3–4), 351–370.
Hall, R. (2012). Late Jurassic–Cenozoic reconstructions of the Indonesian region and the Indian Ocean. *Tectonophysics*, *570*, 1–41.
Harlavan, Y., & Erel, Y. (2002). The release of Pb and REE from granitoids by the dissolution of accessory phases. *Geochimica et Cosmochimica Acta*, *66*(5), 837–848.
Hein, C. J., Galy, V., Galy, A., France-Lanord, C., Kudrass, H., & Schwenk, T. (2017). Post-glacial climate forcing of surface processes in the Ganges–Brahmaputra river basin and implications for carbon sequestration. *Earth and Planetary Science Letters*, *478*, 89–101.
Henrot, A. J., Utescher, T., Erdei, B., Dury, M., Hamon, N., Ramstein, G., et al. (2017). Middle Miocene climate and vegetation models and their validation with proxy data. *Palaeogeography, Palaeoclimatology, Palaeoecology*, *467*, 95–119. https://doi.org/10.1016/j.palaeo.2016.05.026
Hodges, K., Bowring, S., Davidek, K., Hawkins, D., & Krol, M. (1998). Evidence for rapid displacement on Himalayan normal faults and the importance of tectonic denudation in the evolution of mountain ranges. *Geology*, *26*(6), 483.
Hodges, K. V. (2000). Tectonics of the Himalaya and southern Tibet from two perspectives. *GSA Bulletin*, *112*, 324–350.
Holbourn, A., Kuhnt, W., Regenberg, M., Schulz, M., Mix, A., & Andersen, N. (2010). Does Antarctic glaciation force migration of the tropical rain belt? *Geology*, *38*(9), 783–786.
Holbourn, A., Kuhnt, W., Schulz, M., & Erlenkeuser, H. (2005). Impacts of orbital forcing and atmospheric carbon dioxide on Miocene ice-sheet expansion. *Nature*, *438*(7067), 483–487.
Holbourn, A. E., Kuhnt, W., Clemens, S. C., Kochhann, K. G. D., Johnck, J., Lubbers, J., & Andersen, N. (2018). Late Miocene climate cooling and intensification of southeast Asian winter monsoon. *Nature Communications*, *9*(1), 1584.
Hovan, S. A., & Rea, D. K. (1992). The Cenozoic record of continental mineral deposition on broken and Ninetyeast Ridges, Indian Ocean: Southern African aridity and sediment delivery from the Himalayas. *Paleoceanography*, *7*(6), 833–860.
Jacobsen, S. B., & Wasserburg, G. J. (1980). Sm-Nd isotopic evolution of chondrites. *Earth and Planetary Science Letters*, *50*, 139–155.
Jochum, K. P., Weis, U., Schwager, B., Stoll, B., Wilson, S. A., Haug, G. H., et al. (2016). Reference values following ISO guidelines for frequently requested rock reference materials. *Geostandards and Geoanalytical Research*, *40*(3), 333–350. https://doi.org/10.1111/j.1751-908X.2015.00392.x
John, C. M., Karner, G. D., & Mutti, M. (2004). δ18O and Marion Plateau backstripping: Combining two approaches to constrain late middle Miocene eustatic amplitude. *Geology*, *32*(9), 829–832.
Joussain, R., Colin, C., Liu, Z., Meynadier, L., Fournier, L., Fauquembergue, K., et al. (2016). Climatic control of sediment transport from the Himalayas to the proximal NE Bengal Fan during the last glacial-interglacial cycle. *Quaternary Science Reviews*, *148*, 1–16. https://doi.org/10.1016/j.quascirev.2016.06.016
Kellett, D. A., Grujic, D., & Erdmann, S. (2009). Miocene structural reorganization of the south Tibetan detachment, eastern Himalaya: Implications for continental collision. *Lithosphere*, *1*(5), 259–281.
Kessarkar, P. M., Rao, V. P., Ahmad, S., Patil, S., Kumar, A. A., Babu, G. A., et al. (2005). Changing sedimentary environment during the Late Quaternary: Sedimentological and isotopic evidence from the distal Bengal Fan. *Deep Sea Research Part I: Oceanographic Research Papers*, *52*(9), 1591–1615. https://doi.org/10.1016/j.dsr.2005.01.009
Kumar, V. S., Pathak, K., Pednekar, P., Raju, N., & Gowthaman, R. (2006). Coastal processes along the Indian coastline. *Current Science*, 530–536.
LeFort, P. (1975). Himalayas-collided range-present knowledge of continental arc. *American Journal of Science*, *275*(A), 144.
Li, J., Liu, S., Shi, X., Zhang, H., Fang, X., Chen, M.-T., et al. (2018). Clay minerals and Sr-Nd isotopic composition of the Bay of Bengal sediments: Implications for sediment provenance and climate control since 40 ka. *Quaternary International*, *493*, 50–58. https://doi.org/10.1016/j.quaint.2018.06.044
Lightfoot, P., Hawkesworth, C., Devey, C. W., Rogers, N., & Calsteren, P. V. (1990). Source and differentiation of Deccan Trap lavas: Implications of geochemical and mineral chemical variations. *Journal of Petrology*, *31*(5), 1165–1200.
Lübbers, J., Kuhnt, W., Holbourn, A. E., Bolton, C. T., Gray, E., Usui, Y., et al. (2019). The Middle to Late Miocene "carbonate crash" in the equatorial Indian Ocean. *Paleoceanography and Paleoclimatology*, *34*, 813–832. https://doi.org/10.1029/2018PA003482
Mahoney, J., Macdougall, J., Lugmair, G., Murali, A., Das, M. S., & Gopalan, K. (1982). Origin of the Deccan Trap flows at Mahabaleshwar inferred from Nd and Sr isotopic and chemical evidence. *Earth and Planetary Science Letters*, *60*(1), 47–60.
McNeill, L. C., Dugan, B., Backman, J., Pickering, K. T., Pouderoux, H. F. A., Henstock, T. J., et al. (2017). Understanding Himalayan erosion and the significance of the Nicobar Fan. *Earth and Planetary Science Letters*, *475*, 134–142. https://doi.org/10.1016/j.epsl.2017.07.019
Miller, K. G., Browning, J. V., Schmelz, W. J., Kopp, R. E., Mountain, G. S., & Wright, J. D. (2020). Cenozoic sea-level and cryospheric evolution from deep-sea geochemical and continental margin records. *Science Advances*, *6*(20), eaaz1346.
Miller, K. G., Kominz, M. A., Browning, J. V., Wright, J. D., Mountain, G. S., Katz, M. E., et al. (2005). The Phanerozoic record of global sea-level change. *Science*, *310*(5752), 1293–1298. https://doi.org/10.1126/science.1116412
Milliman, J. D., & Syvitski, J. P. (1992). Geomorphic/tectonic control of sediment discharge to the ocean: The importance of small mountainous rivers. *The Journal of Geology*, *100*(5), 525–544.
Millot, R., Allègre, C.-J., Gaillardet, J., & Roy, S. (2004). Lead isotopic systematics of major river sediments: A new estimate of the Pb isotopic composition of the Upper Continental Crust. *Chemical Geology*, *203*(1–2), 75–90.
Molnar, P., & Tapponnier, P. (1978). Active tectonics of Tibet. *Journal of Geophysical Research*, *83*(B11), 5361.
Najman, Y., Bickle, M., Garzanti, E., Pringle, M., Barfod, D., Brozovic, N., et al. (2009). Reconstructing the exhumation history of the Lesser Himalaya, NW India, from a multitechnique provenance study of the foreland basin Siwalik Group. *Tectonics*, *28*, TC5018. https://doi.org/10.1029/2009TC002506
Peucat, J., Vidal, P., Bernard-Griffiths, J., & Condie, K. (1989). Sr, Nd, and Pb isotopic systematics in the Archean low-to high-grade transition zone of southern India: Syn-accretion vs. post-accretion granulites. *The Journal of Geology*, *97*(5), 537–549.
Pickering, K. T., Carter, A., Andò, S., Garzanti, E., Limonta, M., Vezzoli, G., & Milliken, K. L. (2020). Deciphering relationships between the Nicobar and Bengal submarine fans, Indian Ocean. *Earth and Planetary Science Letters*, *544*, 116,329.
Pin, C., & Zalduegui, J. F. S. (1997). Sequential separation of light rare-earth elements, thorium and uranium by miniaturized extraction chromatography: Application to isotopic analyses of silicate rocks. *Analytica Chimica Acta*, *339*, 79–89.
Rao, P. S., Ramaswamy, V., & Thwin, S. (2005). Sediment texture, distribution and transport on the Ayeyarwady continental shelf, Andaman Sea. *Marine Geology*, *216*(4), 239–247.

Raymo, M. E. (1994). The Himalayas, organic carbon burial, and climate in the Miocene. *Paleoceanography*, *9*(3), 399–404.
Raymo, M. E., & Ruddiman, W. F. (1992). Tectonic forcing of late Cenozoic climate. *Nature*, *359*, 117–122.
Robinson, R. A. J., Bird, M., O. O, N. W., Hoey, T., Aye, M. M., Higgitt, D., et al. (2007). The Irrawaddy river sediment flux to the Indian Ocean: The original nineteenth-century data revisited. *The Journal of Geology*, *115*(6), 629–640. https://doi.org/10.1086/521607
Schulz, M., & Mudelsee, M. (2002). REDFIT: Estimating red-noise spectra directly from unevenly spaced paleoclimatic time series. *Computers & Geosciences*, *28*(3), 421–426.
Searle, M. P., Law, R. D., Godin, L., Larson, K. P., Streule, M. J., Cottle, J. M., & Jessup, M. J. (2008). Defining the Himalayan main central thrust in Nepal. *Journal of the Geological Society*, *165*(2), 523–534.
Singh, M., Singh, I. B., & Müller, G. (2007). Sediment characteristics and transportation dynamics of the Ganga River. *Geomorphology*, *86*(1–2), 144–175.
Singh, S. K., & France-Lanord, C. (2002). Tracing the distribution of erosion in the Brahmaputra watershed from isotopic compositions of stream sediments. *Earth and Planetary Science Letters*, *202*, 645–662.
Srinivas, B., & Sarin, M. M. (2013). Atmospheric dry-deposition of mineral dust and anthropogenic trace metals to the Bay of Bengal. *Journal of Marine Systems*, *126*, 56–68.
Steiger, R. H., & Jäger, E. (1977). Subcommission on geochronology: Convention on the use of decay constants in geo- and cosmochronology. *Earth and Planetary Science Letters*, *36*, 359–362.
Sun, Y., An, Z., Clemens, S. C., Bloemendal, J., & Vandenberghe, J. (2010). Seven million years of wind and precipitation variability on the Chinese Loess Plateau. *Earth and Planetary Science Letters*, *297*(3–4), 525–535.
Tanaka, T., Togashi, S., Kamioka, H., Amakawa, H., Kagami, H., Hamamoto, T., et al. (2000). JNdi-1: A neodymium isotopic reference in consistency with LaJolla neodymium. *Chemical Geology*, *168*(3–4), 279–281. https://doi.org/10.1016/S0009-2541(00)00198-4
Thiede, R. C., Bookhagen, B., Arrowsmith, J. R., Sobel, E. R., & Strecker, M. R. (2004). Climatic control on rapid exhumation along the Southern Himalayan Front. *Earth and Planetary Science Letters*, *222*(3–4), 791–806.
Thiede, R. C., Ehlers, T. A., Bookhagen, B., & Strecker, M. R. (2009). Erosional variability along the northwest Himalaya. *Journal of Geophysical Research*, *114*, F01015. https://doi.org/10.1029/2008JF001010
Tremblay, M. M., Fox, M., Schmidt, J. L., Tripathy-Lang, A., Wielicki, M. M., Harrison, T. M., et al. (2015). Erosion in southern Tibet shut down at ~10 Ma due to enhanced rock uplift within the Himalaya. *PNAS*, *112*(39), 12,030–12,035. https://doi.org/10.1073/pnas.1515652112
Tripathy, G. R., Singh, S. K., Bhushan, R., & Ramaswamy, V. (2011). Sr-Nd isotope composition of the Bay of Bengal sediments: Impact of climate on erosion in the Himalaya. *Geochemical Journal*, *45*(3), 175–186.
Tütken, T., Eisenhauer, A., Wiegand, B., & Hansen, B. T. (2002). Glacial-interglacial cycles in Sr and Nd isotopic composition of Arctic marine sediments triggered by the Svalbard/Barents Sea ice sheet. *Marine Geology*, *182*, 351–372.
Unger, D., Ittekkot, V., Schäfer, P., Tiemann, J., & Reschke, S. (2003). Seasonality and interannual variability of particle fluxes to the deep Bay of Bengal: Influence of riverine input and oceanographic processes. *Deep Sea Research Part II: Topical Studies in Oceanography*, *50*(5), 897–923.
Vance, D., & Thirlwall, M. (2002). An assessment of mass discrimination in MC-ICPMS using Nd isotopes. *Chemical Geology*, *185*, 227–240.
Vannay, J.-C., Grasemann, B., Rahn, M., Frank, W., Carter, A., Baudraz, V., & Cosca, M. (2004). Miocene to Holocene exhumation of metamorphic crustal wedges in the NW Himalaya: Evidence for tectonic extrusion coupled to fluvial erosion. *Tectonics*, *23*, TC1014. https://doi.org/10.1029/2002TC001429
White, N. M., Pringle, M., Garzanti, E., Bickle, M. J., Najman, Y., Chapman, H. J., & Friend, P. (2002). Constraints on the exhumation and erosion of the High Himalayan Slab, NW India, from foreland basin deposits. *Earth and Planetary Science Letters*, *195*, 29–44.
White, W. M., Albarède, F., & Télouk, P. (2000). High-precision analysis of Pb isotope ratios by multi-collector ICP-MS. *Chemical Geology*, *167*(3–4), 257–270.
Wilson, D. J., Galy, A., Piotrowski, A. M., & Banakar, V. K. (2015). Quaternary climate modulation of Pb isotopes in the deep Indian Ocean linked to the Himalayan chemical weathering. *Earth and Planetary Science Letters*, *424*, 256–268.
Yin, A. (2006). Cenozoic tectonic evolution of the Himalayan orogen as constrained by along-strike variation of structural geometry, exhumation history, and foreland sedimentation. *Earth-Science Reviews*, *76*(1–2), 1–131.
You, Y., Huber, M., Müller, R. D., Poulsen, C. J., & Ribbe, J. (2009). Simulation of the middle Miocene climate optimum. *Geophysical Research Letters*, *36*, L04702. https://doi.org/10.1029/2008GL036571
Zahirovic, S., Matthews, K. J., Flament, N., Müller, R. D., Hill, K. C., Seton, M., & Gurnis, M. (2016). Tectonic evolution and deep mantle structure of the eastern Tethys since the latest Jurassic. *Earth-Science Reviews*, *162*, 293–337.